Mathematical analysis of the well-posedness of the Hirano active layer concept in 2D models

Deltares

Mathematical analysis of the well-posedness of the Hirano active layer concept in 2D models

1230044

Deltares

Title

Mathematical analysis of the well-posedness of the Hirano active layer concept in 2D models

Client	Project	Reference	Pages
Rijkswaterstaat (WVL)	1230044	1230044-000-ZWS-0035	29

Keywords

Hirano, graded sediment, morphodynamics, eigenvalues, well-posedness, Delft3D

Summary

Morfodynamische simulaties geven belangrijke informatie over het systeemgedrag, en moeten dus van voldoende kwaliteit zijn. Er is aangetoond dat de huidige morfodynamische modellen soms 'elliptisch gedrag' vertonen. Dat betekent dat de resultaten dan mogelijk geen voorspellende waarde meer hebben. Aangezien Rijkswaterstaat veelvuldig gebruik maakt van morfodynamische modellen (bijvoorbeeld bij het project Duurzame Vaardiepte Rijndelta (DVR), maar ook bij het simuleren van de gevolgen van Ruimte voor de Riviermaatregelen en bij ingrepen zoals sedimentsuppletie) is een check op dit probleem noodzakelijk om voldoende vertrouwen te houden in langjarige morfodynamische berekeningen. Vanuit de literatuur en vanuit recent onderzoek van TUD is bekend dat bij bepaalde condities, het actieve laag concept van Hirano dat ten grondslag ligt aan de morfologische modellering van meerdere sediment fracties een elliptisch karakter kan krijgen. Dat ligt niet aan de numerieke modelsystemen (Delft3D en SOBEK) maar is een eigenschap van de wiskundige vergelijkingen. Als men zich niet bewust is van deze eigenschap, is er een risico bij de interpretatie van de resultaten van langjarige morfodynamische berekeningen. Een analyse van dit probleem is urgent en noodzakelijk voor de toepassingen (RWS), voor de adviseurs (o.m. HKV, RHDHV), en ook voor Deltares als adviseur en tevens ontwikkelaar van de numerieke modelsystemen.

In samenwerking tussen TUD, Deltares en RWS kan dit probleem snel opgepakt worden. Door een analyse van het probleem uit te voeren kunnen we aangeven waar de risico's liggen en een oplossingsrichting formuleren die uitzicht biedt op een oplossingsmethode die fundamenteel correct is. Daarmee wordt de richting voor vervolgonderzoek aangegeven. Het bepalen van de aan- of afwezigheid van het probleem (dus: zijn de berekeningen wel of niet elliptisch) in morfodynamische berekeningen die in de praktijk worden gemaakt (bijvoorbeeld bij de beschrijving van de langjarige ontwikkeling van de rivierbodem of het bepalen van de gevolgen van bagger- en suppletieprogramma's) is onderdeel van deze pilotactiviteit.

Version	Date	Author	Initials	Review	Initials	Approval	Initials
1.0 *Revision*: 6886	9-12-2016	Víctor Chavarrías (TU Delft)		Kees Sloff		Johan Boon	
		Willem Ottevanger		Astrid Blom (TU Delft)			

Status

definitief

Contents

Deltares

List of Figures

Deltares

1 Introduction

The current model to predict mixed-sediment river morphodynamics at large spatial scales and long time scales is the active layer model (Hirano, 1971). This is a deterministic model where the bed is discretized in layers and the sediment mixture in a finite number of size fractions. The topmost layer (the active layer) interacts with the flow (i.e., the sediment transport and friction depend on the conditions of this layer) while the layers below (the substrate) only act as bookkeeping system. There is a sediment flux from and to the active layer if there is a time variation of the elevation of the interface between the active layer and the substrate.

This model has proven its value over a wide range of different situations for decades. Nevertheless in some circumstances the model may be ill-posed (Ribberink, 1987; Stecca *et al.*, 2014) and in these conditions produces unphysical and unrealistic results.

There are alternatives to the active layer model as the one by Ribberink (1987) where a second active layer is taken into account. This model was derived for dune-dominated cases and it does not solve the problem of ill-posedness (Sieben, 1997). The continuous model by Blom *et al.* (2003, 2006, 2008) was also derived for dune dominated cases and it is not applicable at large space scales or long time scales (Blom, 2008). A simplified continuous model derived by Viparelli *et al.* (2016) which is applicable at large scale but it can also become ill-posed (Chavarrías *et al.*). Thus the active layer model is still the main model for mixed sediment river morphodynamics.

All previous analyses of the active layer model that we are aware of have been done assuming one-dimensional flow. Yet, to model the effects of flow curvature it is necessary to (at least) consider the bi-dimensionality of flow, which introduces a degree of complexity. While the equations to model the evolution of the bed are intrinsically the same only adding one dimension to the divergence terms, the flow equations substantially change between one and two dimensions. In two dimensions the water flow is modelled using the Shallow Water Equations (which in one dimension reduce into the Saint-Venant (1871) equations). The Shallow Water Equations do not resolve for the vertical distribution of the velocity and are thus inadequate when, for instance, large curvature in a river bend induces a three dimensional flow (secondary flow). Yet, the secondary flow can be parametrized to avoid the expense of a three dimensional model (Kalkwijk and Booij, 1986). The parametrization is based on the intensity of the secondary flow I which is a measure of the magnitude of the velocity component normal to the depth-averaged velocity. An advection-diffusion equation models this variable which is found in extra terms in the momentum equations. Thus, the consideration of secondary flow not only modifies the momentum equations but also adds an extra equation to the system.

Another degree of complexity is added when taking into consideration the effect of the bed slope (in streamwise and lateral direction) in the sediment transport. This effect corrects for the fact that sediment is more easily transported downslope than upslope. A fundamental difference between this second degree of complexity when compared to the parametrization of secondary flow is that this does not introduce a dependent variable as it is modelled as a closure relation. Nevertheless, this closure relation also introduces a diffusive character just as the secondary flow.

Here we aim at building a check function to assess the well-posedness of 2D simulations run in Delft3D. To this end in Section 2 we describe the equations that model shallow water flow coupled to the active layer model. In Section 3 we describe how we characterize a 2D system of partial differential equations and we obtain the matrix-vector formulation of the model. In

Section 4 we present the (preliminary) results of the implementation of the check function.

2 Mathematical Model Description

In this section we describe the equations that model shallow water flow with a parametrized secondary flow correction together with the active layer model of Hirano (1971). These equations represent hydrostatic flow over a mobile bed composed of several (N) non-cohesive sediment fractions. In Section 2.1 we write the model equations. In Section 2.2 we simplify the equations. In Section 2.3 we describe the closure relations of the model.

2.1 Equations

The equations we use are:

- Water mass conservation:

$$\frac{\partial h}{\partial t} + \frac{\partial q_x}{\partial x} + \frac{\partial q_y}{\partial y} = 0 \tag{2.1}$$

- Water momentum conservation in x direction:

$$\frac{\partial q_x}{\partial t} + \frac{\partial (q_x^2/h + gh^2/2)}{\partial x} + \frac{\partial \left(\frac{q_x q_y}{h} \right)}{\partial y} + gh\frac{\partial \eta}{\partial x} - F'_{sx} = -ghS_{fx} \tag{2.2}$$

- Water momentum conservation in y direction:

$$\frac{\partial q_y}{\partial t} + \frac{\partial (q_y^2/h + gh^2/2)}{\partial y} + \frac{\partial \left(\frac{q_x q_y}{h} \right)}{\partial x} + gh\frac{\partial \eta}{\partial y} - F'_{sy} = -ghS_{fy} \tag{2.3}$$

- Constitutive equation for the secondary flow intensity:

$$\frac{\partial I}{\partial t} + \frac{q_x}{h}\frac{\partial I}{\partial x} + \frac{q_y}{h}\frac{\partial I}{\partial y} - D_H\frac{\partial^2 I}{\partial x^2} - D_H\frac{\partial^2 I}{\partial y^2} = S_s \tag{2.4}$$

- Sediment mass conservation for the entire mixture (Exner):

$$\frac{\partial \eta}{\partial t} + \frac{\partial q_{bx}}{\partial x} + \frac{\partial q_{by}}{\partial y} = 0 \tag{2.5}$$

- Sediment mass conservation per grain size in the active layer (Hirano):

$$\frac{\partial M_{ak}}{\partial t} + f_k^I\frac{\partial (\eta - L_a)}{\partial t} + \frac{\partial q_{bkx}}{\partial x} + \frac{\partial q_{bky}}{\partial y} = 0 \quad k \in \{1, N-1\} \tag{2.6}$$

- Sediment mass conservation per grain size in the substrate:

$$\frac{\partial M_{sk}}{\partial t} - f_k^I\frac{\partial (\eta - L_a)}{\partial t} = 0 \quad k \in \{1, N-1\} \tag{2.7}$$

where:

- x = x coordinate $[m]$
- y = y coordinate $[m]$
- t = time coordinate $[s]$
- h = flow depth $[m]$
- q_x = specific water discharge in x direction $[m^2/s]$

- q_y = specific water discharge in y direction $[m^2/s]$
- η = bed elevation $[m]$
- f_k^I = volume fraction content of size fraction k at the interface between the active layer and the substrate $[-]$
- L_a = active layer thickness $[m]$
- q_{bkx} = sediment transport of size fraction k (including pores) in x direction $[m^2/s]$
- q_{bky} = sediment transport of size fraction k (including pores) in y direction $[m^2/s]$
- q_{bx} = total sediment transport (including pores) in x direction $[m^2/s]$
- q_{by} = total sediment transport (including pores) in y direction $[m^2/s]$
- S_{fx} = friction slope in the x direction $[-]$
- S_{fy} = friction slope in the y direction $[-]$
- g = acceleration due to gravity $[m/s^2]$
- $M_{ak} = F_{ak}L_a$ = volume of sediment of size fraction k in the active layer per unit of surface area $[m]$
- F_{ak} = volume fraction content of size fraction k in the active layer $[-]$
- $M_{sk} = \int_{\eta_0}^{\eta-L_a} f_{sk}(z)\mathrm{d}z$ = volume of sediment of size fraction k in the substrate per unit of surface area $[m]$
- η_0 = reference bed elevation $[m]$
- f_{sk} = volume fraction of size fraction k in the substrate $[-]$
- N = number of size fractions $[-]$
- F'_{sx} = force per unit mass along the flow depth due to the secondary flow in the x direction $[m^2/s^2]$
- F'_{sy} = force per unit mass along the flow depth due to the secondary flow in the y direction $[m^2/s^2]$
- I = secondary flow intensity $[m/s]$
- D_H = diffusion coefficient $[m^2/s]$
- S_s = source term $[m/s]$

We use a notation with prime to avoid confusion with the Deltares notation which is based on the non-conservative Shallow Water Equations.

The volume fraction content of sediment at the active layer and the substrate are constrained by the equations:

$$\sum_{k=1}^{N} F_{ak} = 1, \quad \sum_{k=1}^{N} f_{sk}(z) = 1 \;, \tag{2.8}$$

thus, the volume of sediment per unit area are constrained by the equations:

$$\sum_{k=1}^{N} M_{ak} = L_a, \quad \sum_{k=1}^{N} M_{sk} = \eta - L_a - \eta_0 \;. \tag{2.9}$$

2.2 Simplifications

We:

1   assume a constant active layer thickness:

$$\frac{\partial L_a}{\partial t} = 0 \tag{2.10}$$

Substitution of Equation 2.10 in 2.6 and 2.7 yields:

$$\frac{\partial M_{ak}}{\partial t} - f_k^I \frac{\partial q_{bx}}{\partial x} - f_k^I \frac{\partial q_{by}}{\partial y} + \frac{\partial q_{bkx}}{\partial x} + \frac{\partial q_{bky}}{\partial y} = 0 \quad k \in \{1, N-1\} \tag{2.11}$$

$$\frac{\partial M_{sk}}{\partial t} + f_k^I \frac{\partial q_{bx}}{\partial x} + f_k^I \frac{\partial q_{by}}{\partial y} = 0 \quad k \in \{1, N-1\} \tag{2.12}$$

2.3 Closure Relations

The governing equations still need closure relations for the friction slope, the sediment transport rate, the secondary flow terms, and the fractions at the interface between the substrate and the active layer to form a complete set of equations. In this section we describe those closure relations.

2.3.1 Friction Slope

The friction slope is:

$$S_{fx} = \frac{C_f q_x Q}{gh^3} \quad S_{fy} = \frac{C_f q_y Q}{gh^3} \tag{2.13}$$

where:

- C_f = dimensionless friction coefficient $[-]$
- $Q = |\vec{q}|$ = module of the specific water discharge $[m/s^2]$

2.3.2 Sediment Transport Rate

The sediment transport rate per size fraction (including pores) $\vec{q_{bk}}$ $[m^2/s]$ can be expressed as:

$$\vec{q_{bk}} = (q_{bkx}, q_{bky}) = q_{bk}(\cos \varphi_\tau, \sin \varphi_\tau) \quad k \in \{1, N\} \tag{2.14}$$

where:

- φ_τ = direction of the sediment transport rate [rad]
- q_{bk} = absolute value of the sediment transport rate including pores $[m^2/s]$

The direction of the sediment transport rate φ_τ [rad] is:

$$\tan \varphi_\tau = \frac{q_y - h\alpha_I \frac{q_x}{Q} I}{q_x - h\alpha_I \frac{q_y}{Q} I} \tag{2.15}$$

where:

- α_I = constant $[-]$

The constant α_I $[-]$ is:

$$\alpha_I = \frac{2}{\kappa^2} E_s \left(1 - \frac{\sqrt{C_f}}{2\kappa}\right) \tag{2.16}$$

where:

- κ = Von Kármán constant $[-]$
- E_s = calibration parameter $[-]$

The absolute value of the sediment transport rate is:

$$q_{bk} = F_{ak} \sqrt{gRd_k^3} \, (1-p) \, A \max\left(\theta_k - \xi_k \theta_c, 0\right)^B \quad k \in \{1, N\} \tag{2.17}$$

where:

- p = porosity $[-]$
- $R = \rho_s/\rho_w - 1$ = submerged sediment density $[-]$
- $\rho_s = 2650$ = sediment density $[kg/m^3]$
- $\rho_w = 1000$ = water density $[kg/m^3]$
- d_k = characteristic grain size of size fraction k $[m]$
- A = nondimensional parameter $[-]$
- B = nondimensional parameter $[-]$
- θ_k = module of the Shields stress of size fraction k [-]
- θ_c = nondimensional critical bed shear stress $[-]$
- ξ_k = hiding coefficient $[-]$

The module of the Shields stress is:

$$\theta_k = \frac{C_f \left(\frac{Q}{h}\right)^2}{gRd_k} \quad k \in \{1, N\} \tag{2.18}$$

A common hiding functions is the one due to Egiazaroff (1965):

$$\xi_k = \left(\frac{\log_{10}(19)}{\log_{10}\left(19\frac{d_k}{D_m}\right)}\right)^2 \quad k \in \{1, N\} \tag{2.19}$$

where:

- D_m = characteristic mean grain size of the mixture $[m]$

A simpler expression was developed by Parker *et al.* (1982):

$$\xi_k = \left(\frac{D_m}{d_k}\right)^b \quad k \in \{1, N\} \tag{2.20}$$

where:

- b = nondimensional parameter $[-]$

2.3.3 Secondary Flow Terms

The secondary flow terms in the momentum equations are:

$$F'_{sx} = \frac{\partial T'_{xx}}{\partial x} + \frac{\partial T'_{xy}}{\partial y} \tag{2.21}$$

$$F'_{sy} = \frac{\partial T'_{yx}}{\partial x} + \frac{\partial T'_{yy}}{\partial y} \tag{2.22}$$

where:

- T'_{lm} = shear stress per unit mass and volume along the flow depth in the direction l-m $[m^3/s^2]$

The closure relation for the secondary flow terms are:

$$T'_{xx} = -2\frac{\beta^* I}{Q} q_x q_y \tag{2.23}$$

$$T'_{xy} = T'_{yx} = \frac{\beta^* I}{Q}\left(q_x^2 - q_y^2\right) \tag{2.24}$$

$$T'_{yy} = T'_{yy} = 2\frac{\beta^* I}{Q} q_x q_y \tag{2.25}$$

where:

- $\beta^* = \beta_c\left(5\alpha - 15.6\alpha^2 + 37.5\alpha^3\right)$ = constant $[-]$
- $\beta_c \in [0, 1]$ = calibration parameter $[-]$
- $\alpha = \frac{\sqrt{C_f}}{\kappa} < 0.5$ = constant $[-]$

2.3.4 Volume Fraction Content at the Interface

The volume fraction content at the interface between the active layer and the substrate under degradational conditions is assumed to be equal to the volume fraction content at the top part of the substrate. Under aggradational conditions Hirano (1971) proposed the flux to the substrate to have the same grain size distribution as the active layer. Parker (1991) introduced the concept that the aggradational flux to the substrate is also influenced by the grain size distribution of the bed load. Hoey and Ferguson (1994) combined both concepts in a parameter that sets the contribution of the bed load relative to the active layer. Currently, only the initial concept of Hirano is implemented in Delft3D which in mathematical terms can be written as:

$$f_k^I = \begin{cases} f_{sk}(z = \eta - L_a) & \text{if} \quad \frac{\partial(\eta - L_a)}{\partial t} < 0 \\ F_{ak} & \text{if} \quad \frac{\partial(\eta - L_a)}{\partial t} > 0 \end{cases} \tag{2.26}$$

Mathematical analysis of the well-posedness of the Hirano active layer concept in 2D models

3 Model Characterization

In this section we describe the assessment of the model comprised by the Shallow Water Equations coupled to the active layer model Hirano (1971). In Section 3.1 we introduce the necessary mathematical concepts. To asses the model we decompose the equations' terms into spatial gradients of the dependent variables (Section 3.2). In Section 3.3 we present the matrix-vector formulation of the model.

3.1 Hyperbolicity of a 2D System of Equations

We first assume a system of equations without diffusive terms. In a 1D problem the equations can be recast in a matrix form:

$$\frac{\partial \mathbf{Q}}{\partial t} + \mathbf{A}\frac{\partial \mathbf{Q}}{\partial x} = \mathbf{S} \ . \tag{3.1}$$

This is the one-dimensional quasi-linear non-conservative form of the advection equation. $\mathbf{Q}$ is the vector of dependent variables, $\mathbf{A}$ is the system matrix, and $\mathbf{S}$ is the vector of source terms. $t\ [s]$ denotes the time coordinate, $x\ [m]$ the streamwise coordinate.

The problem in Equation 3.1 will be well-posed if wave-like solutions exist. This is, if the n system equations give rise to n waves propagating along the domain. This property is called hyperbolicity. A system is hyperbolic or parabolic at a point (x, t) if all the eigenvalues of matrix $\mathbf{A}$ are real. Physical propagation problems are modelled with hyperbolic or parabolic systems of equations. If all the eigenvalues are complex, the system is said to be elliptic. Elliptic systems model equilibrium physical problems. If matrix $\mathbf{A}$ has both real and complex eigenvalues it is a mixed-type system.

A 2D problem can be recast in a matrix form:

$$\frac{\partial \mathbf{Q}}{\partial t} + \mathbf{A_x}\frac{\partial \mathbf{Q}}{\partial x} + \mathbf{A_y}\frac{\partial \mathbf{Q}}{\partial y} = \mathbf{S} \tag{3.2}$$

where $\mathbf{A_x}$ and $\mathbf{A_y}$ are the system matrices in x and y direction.

For a 2D problem to be hyperbolic, wavelike solutions must exist for any arbitrary direction specified by the unit vector $\vec{n} = (n_x, n_y)$. Thus, the problem specified by Equation 3.2 is said to be hyperbolic if the matrix:

$$\mathbf{A_{2D}} = \mathbf{A_x}n_x + \mathbf{A_y}n_y \tag{3.3}$$

diagonalizes with real eigenvalues. In this case, the derivative of the eigenvalues with respect to n_x and n_y yield the eigenvalues in the x-y domain. These eigenvalues form the intersection of the Monge cone(s) with a unit time (see e.g. Sloff (1992); Sieben (1994)). Thus the Monge cone is a visualization of the propagation celerity of the information in the domain. If at least one cone is not real the system is elliptic.

3.2 Decomposition of the System Equations

In this section we decompose the divergence terms of the model equations.

3.2.1 Decomposition of the Sediment Transport Rate

The directional sediment transport rates q_{bkx} and q_{bky} are not only a function of the flow velocity in their respective directions but also of the flow velocity in the other direction and the secondary flow intensity:

$$q_{bkx} = f(h, q_x, q_y, I, M_{ak}) \Rightarrow$$

$$\Rightarrow \frac{\partial q_{bkx}}{\partial x} = \frac{\partial q_{bkx}}{\partial h}\frac{\partial h}{\partial x} + \frac{\partial q_{bkx}}{\partial q_x}\frac{\partial q_x}{\partial x} + \frac{\partial q_{bkx}}{\partial q_y}\frac{\partial q_y}{\partial x} + \frac{\partial q_{bkx}}{\partial I}\frac{\partial I}{\partial x}$$

$$+ \sum_{l=1}^{N-1} \frac{\partial q_{bkx}}{\partial M_{al}}\frac{\partial M_{al}}{\partial x} \quad k \in \{1, N\} \tag{3.4}$$

and,

$$q_{bky} = f(h, q_x, q_v, I, M_{ak}) \Rightarrow$$

$$\Rightarrow \frac{\partial q_{bky}}{\partial y} = \frac{\partial q_{bky}}{\partial h}\frac{\partial h}{\partial y} + \frac{\partial q_{bky}}{\partial q_x}\frac{\partial q_x}{\partial y} + \frac{\partial q_{bky}}{\partial q_y}\frac{\partial q_y}{\partial y} + \frac{\partial q_{bky}}{\partial I}\frac{\partial I}{\partial y}$$

$$+ \sum_{l=1}^{N-1} \frac{\partial q_{bky}}{\partial M_{al}}\frac{\partial M_{al}}{\partial y} \quad k \in \{1, N\} \tag{3.5}$$

The same holds for the total bed load in x and y direction (q_{bx} and q_{by}). Note that M_{aN} is not an independent variable.

The derivatives of the directional sediment transport rates with respect to the model variables have the same expression as when secondary flow is not considered. However, in this case the direction of the sediment transport depends on all the variables but the volume of sediment in the active layer. Thus, some of the derivatives of the sediment transport direction that are zero when secondary flow is not considered are not 0 when this is considered.

3.2.2 Secondary Flow Terms

The secondary flow t, Equations (2.23), (2.24), and (2.24) are a function of the specific water discharge and secondary flow intensity only:

$$T'_{ij} = f(q_x, q_y, I) \Rightarrow$$

$$\Rightarrow \frac{\partial T'_{ij}}{\partial x} = \frac{\partial T'_{ij}}{\partial q_x}\frac{\partial q_x}{\partial x} + \frac{\partial T'_{ij}}{\partial q_y}\frac{\partial q_y}{\partial x} + \frac{\partial T'_{ij}}{\partial I}\frac{\partial I}{\partial x}$$

and $$\tag{3.6}$$

$$\Rightarrow \frac{\partial T'_{ij}}{\partial y} = \frac{\partial T'_{ij}}{\partial q_x}\frac{\partial q_x}{\partial y} + \frac{\partial T'_{ij}}{\partial q_y}\frac{\partial q_y}{\partial y} + \frac{\partial T'_{ij}}{\partial I}\frac{\partial I}{\partial y}$$

where $i = (x, y)$ and $j = (x, y)$.

3.2.3 Substitution and Expansion

In this section we substitute the decomposed divergence terms in the model equations and we expand the terms to obtain products of the gradient of the dependent variables.

All the terms in the water mass equation, Equation (2.1), are already products of the gradient of the dependent variables.

Expanding the terms of the equation for the conservation of water momentum in the x direction, Equation (2.2), we obtain:

$$
\begin{aligned}
\frac{\partial q_x}{\partial t} + \left(gh - \left(\frac{q_x}{h}\right)^2 \right) \frac{\partial h}{\partial x} - \frac{q_x q_y}{h^2} \frac{\partial h}{\partial y} \\
+ \left(2\frac{q_x}{h} - \frac{\partial T'_{xx}}{\partial q_x} \right) \frac{\partial q_x}{\partial x} + \left(\frac{q_y}{h} - \frac{\partial T'_{xy}}{\partial q_x} \right) \frac{\partial q_x}{\partial y} \\
- \frac{\partial T'_{xx}}{\partial q_y} \frac{\partial q_y}{\partial x} + \left(\frac{q_x}{h} - \frac{\partial T'_{xy}}{\partial q_y} \right) \frac{\partial q_y}{\partial y} \\
- \frac{\partial T'_{xx}}{\partial I} \frac{\partial I}{\partial x} - \frac{\partial T'_{xy}}{\partial I} \frac{\partial I}{\partial y} + gh\frac{\partial \eta}{\partial x} = -ghS_{fx}
\end{aligned}
\tag{3.7}
$$

Expanding the terms of the equation for the conservation of water momentum in the y direction, Equation (2.3), we obtain:

$$
\begin{aligned}
\frac{\partial q_y}{\partial t} - \frac{q_x q_y}{h^2} \frac{\partial h}{\partial x} + \left(gh - \left(\frac{q_y}{h}\right)^2 \right) \frac{\partial h}{\partial y} \\
+ \left(\frac{q_y}{h} - \frac{\partial T'_{yx}}{\partial q_x} \right) \frac{\partial q_x}{\partial x} - \frac{\partial T'_{yy}}{\partial q_x} \frac{\partial q_x}{\partial y} \\
+ \left(\frac{q_x}{h} - \frac{\partial T'_{yx}}{\partial q_y} \right) \frac{\partial q_y}{\partial x} + \left(2\frac{q_y}{h} - \frac{\partial T'_{yy}}{\partial q_y} \right) \frac{\partial q_y}{\partial y} \\
- \frac{\partial T'_{yx}}{\partial I} \frac{\partial I}{\partial x} - \frac{\partial T'_{yy}}{\partial I} \frac{\partial I}{\partial y} + gh\frac{\partial \eta}{\partial y} = -ghS_{fy}
\end{aligned}
\tag{3.8}
$$

All the terms in the constitutive equation of the secondary flow intensity, Equation (2.4), are already products of the gradient of the dependent variables.

Substitution of equations 3.4, and 3.5 in 2.5 yields the Exner equation:

$$
\begin{aligned}
\frac{\partial \eta}{\partial t} + \frac{\partial q_{bx}}{\partial h} \frac{\partial h}{\partial x} + \frac{\partial q_{bx}}{\partial q_x} \frac{\partial q_x}{\partial x} + \frac{\partial q_{bx}}{\partial q_y} \frac{\partial q_y}{\partial x} + \frac{\partial q_{bx}}{\partial I} \frac{\partial I}{\partial x} + \sum_{l=1}^{N-1} \frac{\partial q_{bx}}{\partial M_{al}} \frac{\partial M_{al}}{\partial x} \\
+ \frac{\partial q_{by}}{\partial h} \frac{\partial h}{\partial y} + \frac{\partial q_{by}}{\partial q_x} \frac{\partial q_x}{\partial y} + \frac{\partial q_{by}}{\partial q_y} \frac{\partial q_y}{\partial y} + \frac{\partial q_{by}}{\partial I} \frac{\partial I}{\partial y} + \sum_{l=1}^{N-1} \frac{\partial q_{by}}{\partial M_{al}} \frac{\partial M_{al}}{\partial y} = 0
\end{aligned}
\tag{3.9}
$$

Substitution of equations 3.4, and 3.5 in 2.11 yields the Hirano equation:

$$
\begin{aligned}
\frac{\partial M_{ak}}{\partial t} &+ \left(\frac{\partial q_{bkx}}{\partial h} - f_k^I \frac{\partial q_{bx}}{\partial h}\right)\frac{\partial h}{\partial x} + \left(\frac{\partial q_{bkx}}{\partial q_x} - f_k^I \frac{\partial q_{bx}}{\partial q_x}\right)\frac{\partial q_x}{\partial x} \\
&+ \left(\frac{\partial q_{bkx}}{\partial q_y} - f_k^I \frac{\partial q_{bx}}{\partial q_y}\right)\frac{\partial q_y}{\partial x} + \left(\frac{\partial q_{bkx}}{\partial I} - f_k^I \frac{\partial q_{bx}}{\partial I}\right)\frac{\partial I}{\partial x} \\
&+ \sum_{l=1}^{N-1}\left(\frac{\partial q_{bkx}}{\partial M_{al}} - f_k^I \frac{\partial q_{bx}}{\partial M_{al}}\right)\frac{\partial M_{al}}{\partial x} \\
&+ \left(\frac{\partial q_{bky}}{\partial h} - f_k^I \frac{\partial q_{by}}{\partial h}\right)\frac{\partial h}{\partial y} + \left(\frac{\partial q_{bky}}{\partial q_x} - f_k^I \frac{\partial q_{by}}{\partial q_x}\right)\frac{\partial q_x}{\partial x} \\
&+ \left(\frac{\partial q_{bky}}{\partial q_y} - f_k^I \frac{\partial q_{by}}{\partial q_y}\right)\frac{\partial q_y}{\partial y} + \left(\frac{\partial q_{bky}}{\partial I} - f_k^I \frac{\partial q_{by}}{\partial I}\right)\frac{\partial I}{\partial y} \\
&+ \sum_{l=1}^{N-1}\left(\frac{\partial q_{bky}}{\partial M_{al}} - f_k^I \frac{\partial q_{by}}{\partial M_{al}}\right)\frac{\partial M_{al}}{\partial y} = 0 \quad k \in \{1, N-1\}
\end{aligned}
\tag{3.10}
$$

3.3 Matrix-Vector Formulation

Equation (2.12) is a linear combination of equations (2.11) and (2.5). The rest of the equations do not depend on M_{sk}.

We recast the model Equations, (2.1), (3.7), (3.8), (2.4), (3.9), and (3.10) in matrix form:

$$
\frac{\partial \mathbf{Q}}{\partial t} + \mathbf{A_x}\frac{\partial \mathbf{Q}}{\partial x} + \mathbf{A_y}\frac{\partial \mathbf{Q}}{\partial y} + \mathbf{D_x}\frac{\partial^2 \mathbf{Q}}{\partial x^2} + \mathbf{D_y}\frac{\partial^2 \mathbf{Q}}{\partial y^2} + \mathbf{B} = 0
\tag{3.11}
$$

The dependent variables are h, q_x, q_y, I, η, and M_{ak} for $1 \leq k \leq N-1$:

$$
\mathbf{Q} = \begin{bmatrix} h \\ q_x \\ q_y \\ I \\ \eta \\ [M_{ak}] \end{bmatrix}
\tag{3.12}
$$

The system matrix in x direction is:

$$
\mathbf{A}_x = \left[\begin{array}{ccccc|c}
0 & 1 & 0 & 0 & 0 & [0] \\
gh - \left(\frac{q_x}{h}\right)^2 & 2\frac{q_x}{h} - \frac{\partial T'_{xx}}{\partial q_x} & -\frac{\partial T'_{xx}}{\partial q_y} & -\frac{\partial T'_{xx}}{\partial I} & gh & [0] \\
\frac{-q_x q_y}{h^2} & \frac{q_y}{h} - \frac{\partial T'_{yx}}{\partial q_x} & \frac{q_x}{h} - \frac{\partial T'_{yx}}{\partial q_y} & -\frac{\partial T'_{yx}}{\partial I} & 0 & [0] \\
0 & 0 & 0 & \frac{q_x}{h} & 0 & [0] \\
\frac{\partial q_{bx}}{\partial h} & \frac{\partial q_{bx}}{\partial q_x} & \frac{\partial q_{bx}}{\partial q_y} & \frac{\partial q_{bx}}{\partial I} & 0 & \left[\frac{\partial q_{bx}}{\partial M_{al}}\right] \\
\hline
\left[\frac{\partial q_{bkx}}{\partial h} - f_k^I \frac{\partial q_{bx}}{\partial h}\right] & \left[\frac{\partial q_{bkx}}{\partial q_x} - f_k^I \frac{\partial q_{bx}}{\partial q_x}\right] & \left[\frac{\partial q_{bkx}}{\partial q_y} - f_k^I \frac{\partial q_{bx}}{\partial q_y}\right] & \left[\frac{\partial q_{bkx}}{\partial I} - f_k^I \frac{\partial q_{bx}}{\partial I}\right] & [0] & \left[\frac{\partial q_{bkx}}{\partial M_{al}} - f_k^I \frac{\partial q_{bx}}{\partial M_{al}}\right]
\end{array}\right]
\tag{3.13}
$$

The system matrix in y direction is:

$$
\mathbf{A}_y = \left[
\begin{array}{ccccc|c}
0 & 0 & 1 & 0 & 0 & [0] \\
\dfrac{-q_x q_y}{h^2} & \dfrac{q_y}{h} - \dfrac{\partial T'_{xy}}{\partial q_x} & \dfrac{q_x}{h} - \dfrac{\partial T'_{xy}}{\partial q_y} & -\dfrac{\partial T'_{xy}}{\partial I} & 0 & [0] \\
gh - \left(\dfrac{q_y}{h}\right)^2 & -\dfrac{\partial T'_{yy}}{\partial q_x} & 2\dfrac{q_y}{h} - \dfrac{\partial T'_{yy}}{\partial q_y} & -\dfrac{\partial T'_{yy}}{\partial I} & gh & [0] \\
0 & 0 & 0 & \dfrac{q_y}{h} & 0 & [0] \\
\dfrac{\partial q_{by}}{\partial h} & \dfrac{\partial q_{by}}{\partial q_x} & \dfrac{\partial q_{by}}{\partial q_y} & \dfrac{\partial q_{by}}{\partial I} & 0 & \left[\dfrac{\partial q_{by}}{\partial M_{al}}\right] \\ \hline
\left[\dfrac{\partial q_{bky}}{\partial h} - f_k^I \dfrac{\partial q_{by}}{\partial h}\right] & \left[\dfrac{\partial q_{bky}}{\partial q_x} - f_k^I \dfrac{\partial q_{by}}{\partial q_x}\right] & \left[\dfrac{\partial q_{bky}}{\partial q_y} - f_k^I \dfrac{\partial q_{by}}{\partial q_y}\right] & \left[\dfrac{\partial q_{bky}}{\partial I} - f_k^I \dfrac{\partial q_{by}}{\partial I}\right] & [0] & \left[\dfrac{\partial q_{bky}}{\partial M_{al}} - f_k^I \dfrac{\partial q_{by}}{\partial M_{al}}\right]
\end{array}
\right]
$$

$$(3.14)$$

The diffusive matrix in x and y direction are:

$$
\mathbf{D_x} = \mathbf{D_y} = \left[
\begin{array}{ccccc|c}
0 & 0 & 0 & 0 & 0 & [0] \\
0 & 0 & 0 & 0 & 0 & [0] \\
0 & 0 & 0 & 0 & 0 & [0] \\
0 & 0 & 0 & D_H & 0 & [0] \\
0 & 0 & 0 & 0 & 0 & [0] \\ \hline
[0] & [0] & [0] & [0] & [0] & [0]
\end{array}
\right]
\tag{3.15}
$$

The vector of source terms is:

$$
\mathbf{B} = \left[
\begin{array}{c}
0 \\
-ghS_{fx} \\
-ghS_{fy} \\
S_s \\
0 \\ \hline
[0]
\end{array}
\right]
\tag{3.16}
$$

3.4 Implementation in Delft3D

In this section a short description of the implementation of the Hirano check in Delft3D is given. For details about the files and the generated output see Appendix A.

In the current implementation in Delft3D the entries of the Jacobian matrices, Equations (3.13) and (3.14), have been computed numerically. However, the effect of secondary flow and gravitational pull on the sediment in transport have been neglected.

The entries of the Jacobian in top left block (3x3 related to h, q_x and q_y) are directly computed based on the analytical expressions presented in Equations 3.13 and 3.14. The entries of the Jacobian of the other blocks (related to η and M_{ak}) contain derivatives of the sediment transport rate with respect to h, q_x, q_y, and M_{ak}. These derivatives are obtained using using a finite difference approach:

$$
\frac{\partial q_{bkx}}{\partial f} = \frac{q_{bkx}\left(f + \mathrm{d}f\right) - q_{bkx}\left(f\right)}{\mathrm{d}f} ,
\tag{3.17}
$$

where f is one of the dependent variables. To compute these values many calls are made to the sediment transport computation without bed or composition update. For each variable a perturbation $(\mathrm{d}f)$ is introduced. This leads to the following sequence of calls (only the resulting x-direction is shown here, but the y-direction is also computed in the same loop):

- Call 1: perturbation to the first dependent variable:
  $h + \mathrm{d}h, q_x, q_y, \eta, M_{a,1}, \ldots, M_{a,N-1}$
  $\rightarrow q_{bx}(h + \mathrm{d}h), q_{bx,1}(h + \mathrm{d}h) \ldots q_{bx,N-1}(h + \mathrm{d}h)$

- Call 2: perturbation to the second dependent variable:
  $h, q_x + \mathrm{d}q_x, q_y, \eta, M_{a,1}, \ldots, M_{a,N-1}$
  $\rightarrow q_{bx}(q_x + \mathrm{d}q_x), q_{bx,1}(q_x + \mathrm{d}q_x) \ldots q_{bx,N-1}(q_x + \mathrm{d}q_x)$
  $\vdots$

- Call $N + 3$: perturbation to the $N + 3$ (and last) dependent variable:
  $h, q_x, q_y, \eta, M_{a,1}, \ldots, M_{a,N-1} + \mathrm{d}M_{a,N-1}$
  $\rightarrow q_{bx}(M_{a,N-1} + \mathrm{d}M_{a,N-1}), q_{bx,1}(M_{a,N-1} + \mathrm{d}M_{a,N-1}) \ldots q_{bx,N-1}(M_{a,N-1} + \mathrm{d}M_{a,N-1})$

- Call $N + 4$: no perturbation, update of bed elevation and composition:
  $h, q_x, q_y, \eta, M_{a,1}, \ldots, M_{a,N-1}$
  $\rightarrow q_{bx}, q_{bx,1} \ldots q_{bx,N-1}$

To compute the partial derivatives the differentials need to modify only one of the dependent variables at a time. Note that we have chosen to use as dependent variables h, q_x, q_y, η, and M_{ak} for $k = 1, N$. Thus, when a differential is added to, for instance, the flow depth h, we need to impose that there is no change in the specific water discharge in x and y direction by adjusting the mean flow velocity.

In the case of the differentials added to the volume of each sediment fraction in the active layer the constrain that the addition of the volume fraction content of all the sediment in the active layer is equal to 1 (Equations (2.8) and (2.9)) needs to hold. To this end the volume fraction of sediment in the active layer after one size fraction is perturbed (superscript $'$) is added to compute the volume of sediment of the last fraction N as:

$$M'_{aN} = L_a - \sum_{k=1}^{N-1} M'_{ak} \,. \tag{3.18}$$

A series of tests were consequently run during the development after every change to the code, to ensure that the implemented code does not interfere with the normal computation loop. During the development no changes to the outcome of the standard Delft3D simulation were made.

4 Results

4.1 2D Eigenvalue Analysis

In this section we describe the eigenvalue analysis performed to be able to check the implementation of the ellipticity check tool in Delft3D. Once the function is implemented in Delft3D we will compare the eigenvalues obtained by that function to the ones obtained by means of a symbolic solver. The use of the symbolic solver allows us to obtain the eigenvalues without introducing the complexities of the interpolation and the numerical computation of the necessary derivatives in Delft3D. Moreover, we validate the symbolic results with previous analysis and analytical solutions.

Using the symbolic solver of Matlab we obtain a symbolic expression of the system matrix $\mathbf{A}_{2D}$, Equation 3.3, for 4 simplified cases:

1 The Shallow Water Equations without secondary flow correction
2 The Shallow Water Equations without secondary flow correction coupled to the Exner (1920) model (unisize)
3 The Shallow Water Equations without secondary flow correction coupled to the Hirano (1971) model (2 size fractions)
4 The Shallow Water Equations without secondary flow correction coupled to the Hirano (1971) model (3 size fractions)

We obtain the symbolic expressions of eigenvalues of $\mathbf{A}_{2D}$, Equation 3.3, for each case. These expressions are symbolically derived with respect to n_x and n_y to obtain the eigenvalues in x and y coordinates. The evaluation of these last eigenvalues for certain values of unitary vectors covering all the space domain yield the Monge cone associated with each system.

To validate our method we compare the Monge cones obtained using our method to analytical solutions and previous results.

We first consider a case in which $u = 1\ m/s$, $v = 0\ m/s$, and $h = 1\ m$. In Figure 4.1a we plot the intersection of the Monge cone of the Shallow Water Equations at $t = 1\ s$ for this specific case. Note that because we do not consider the non-linearities of the system the time at which we plot the Monge cone is irrelevant. This solution is the same as obtained analytically (Sloff, 1992).

We consider the same situation with a mobile bed composed of one sediment size fraction with characteristic grain size equal to 0.001 m and a dimensionless friction coefficient equal to 0.007. The sediment transport is computed using the relation by Engelund and Hansen (1967). In Figure 4.1b we plot the intersection of the Monge cones of the Shallow Water Equations coupled to the Exner (1920) equation at $t = 1\ s$ for this specific case. Note that a new cone appears close to the origin. A zoom in this cone is plotted in Figure 4.1c. This result is the same as obtained in (Sloff, 1992).

We consider the previous situation in which, rather than one single size fraction, we have two size fractions with characteristic grain sizes equal to 0.001 and 0.002 m. The volume fraction content of both size fractions in the active layer is equal to 0.5. The volume fraction content of both size fractions at the interface between the active layer and the substrate is equal to 0.5. Thus, this situation represents an aggradational case. The active layer thickness is equal
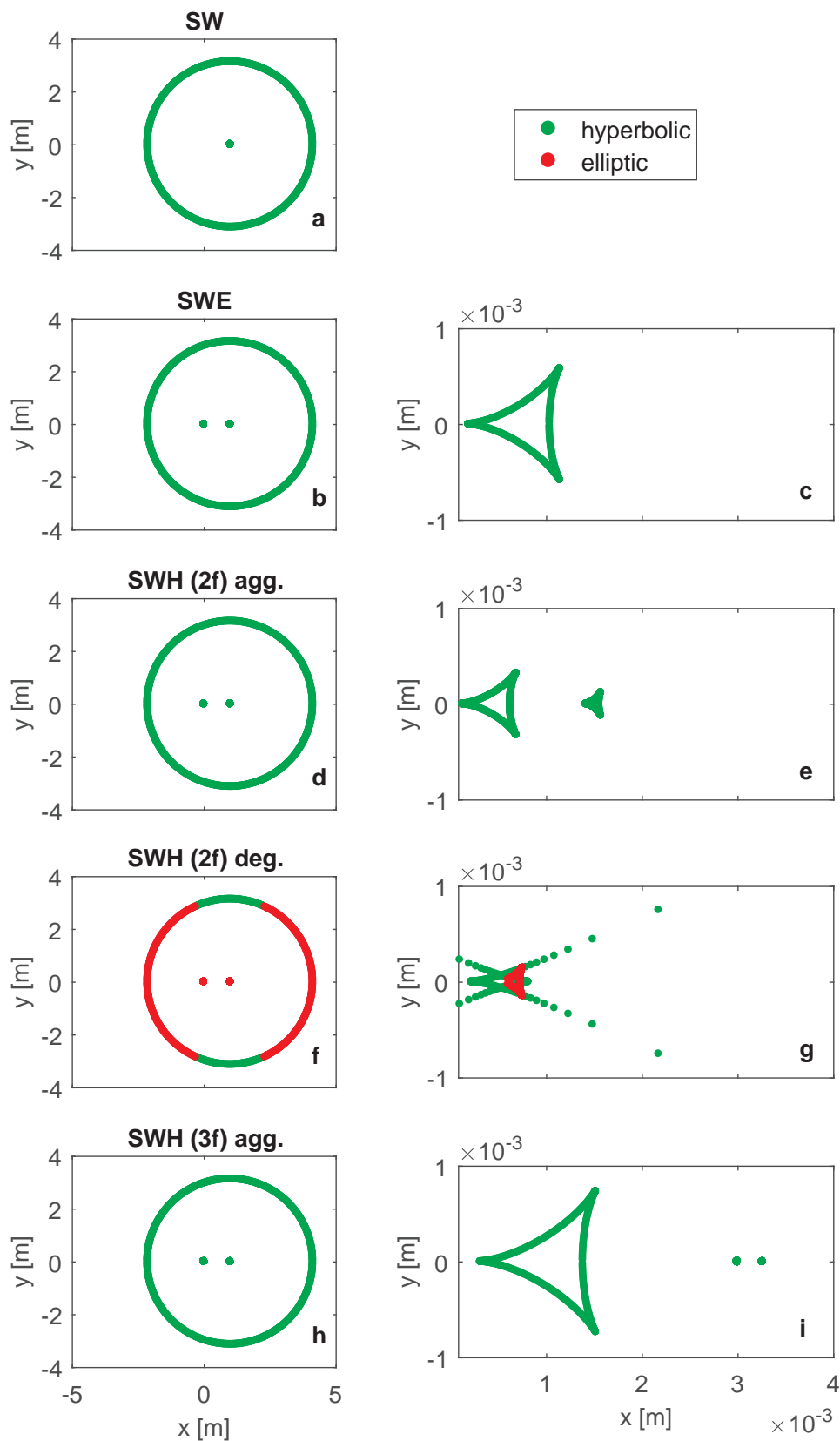
Figure 4.1: *Intersection of the Monge cone at $t = 1\ s$ for the Shallow Water equations in combination with: (**a**) a fixed bed, (**b**-**c**) the Exner (1920) equation, (**d**-**e**) the Hirano (1971) equation considering 2 sediment size fractions in aggradational conditions, (**f**-**g**) the Hirano (1971) equation considering 2 sediment size fractions in degradational conditions, and (**h**-**i**) the Hirano (1971) equation considering 3 sediment size fractions in aggradational conditions.*

to 0.1 m. In Figure 4.1d we plot the intersection of the Monge cones of the Shallow Water Equations coupled to the Hirano (1971) equation at $t = 1\ s$ for this specific case. A new cone appears close to the origin which can only be appreciated if we zoom in (Figure 4.1e). This result is the same as obtained in Sieben (1994).

We consider a situation with the same parameters as before, yet the active layer is composed of the coarse size fraction only and the volume fraction content of fine sediment at the interface between the active layer and the substrate is equal to 1. Thus, this situation represents a degradational case into a fine substrate. In Figure 4.1g we plot a zoom of the intersection of the Monge cone of the Shallow Water Equations coupled to the Hirano equations at $t = 1\ s$ for this specific case. In this case the cone does not pertain to the real numbers. Thus, this situation is elliptic and we can only plot the real part of the cone.

Eventually, we consider the previous situation in which, rather than two size fractions, we have three size fractions with characteristic grain sizes equal to 0.001, 0.002, and 0.004 m. The volume fraction content all size fractions in the active layer is equal to 0.33. The volume fraction content of all size fractions at the interface between the active layer and the substrate is equal to 0.33. Thus, this situation represents an aggradational case. The sediment transport rate is computed using the relation by Meyer-Peter and Müller (1948) with the hiding correction by Parker *et al.* (1982) with parameter b=0.8. In Figure 4.1h we plot the intersection of the Monge cones of the Shallow Water Equations coupled to the Hirano (1971) equation at $t = 1$ s for this specific case. A new cone appears close to the origin which can only be appreciated if we zoom in (Figure 4.1i).

4.2 Implementation Test

In this section we test the implementation of the routine in Delft3D. To this end we compare the matrices given by Deft3D to the ones obtained in the external Matlab algorithm. We test the implementation in three short normal flow simulations which reproduce the last three cases described in Section 4.1.

The domain is 1 m long and 1 m wide, discretized in square cells of side 0.5 m. The boundaries at $x = 0\ m$ and $x = 1\ m$ are open. The boundaries at $y = 0\ m$ and $y = 1\ m$ are closed. To obtain a mean flow velocity in the x direction equal to 1 m/s and 0 m/s in the y direction in combination with a mean flow depth equal to 1 m, the water discharge is equal to 1 m^3/s. The water level at the downstream end is such that the flow depth is equal to 1 m. A tiny lowering of 0.001 m/min is imposed to guarantee that there is a minimal degradation so that the volume fraction content at the interface between the active layer and the substrate is equal to the volume fraction content at the substrate. The nondimensional friction coefficient is equal to 0.007 (Chézy equal to 37.44 $m^{1/2}/s$). The active layer thickness is equal to 0.1 m. The substrate is 1 m deep discretized in two equal layers. Secondary flow is not taken into account. The time step is equal to 0.1 s (which guarantees a small enough CFL number). The simulations last for 60 s.

The matrices in Delft3D are obtained at the node $n = 2$ and $m = 2$ at $t = 2\ s$.

In Simulation 1, the sediment mixture is discretized in two sediment size fractions with characteristic grain sizes equal to 0.001 and 0.002 m. The sediment transport rate is computed using the Engelund and Hansen (1967) sediment transport relation. The sediment input at the upstream end of the fine and coarse size fractions is equal to $5.588 \cdot 10^{-5}$ and $2.794 \cdot 10^{-5}$ m^3/s. This boundary condition is in equilibrium with a bed slope equal to $7.13541 \cdot 10^{-4}$ and a volume fraction content of the fine sediment in the active layer equal to 0.5. The volume fraction content of fine sediment in the substrate is equal to 0.5.

Under these conditions, matrix $\mathbf{A}_x$, Equation 3.13, and $\mathbf{A}_y$, Equation 3.14, (assuming no secondary flow) computed in Matlab are:

$$\mathbf{A}_{x1} = \begin{bmatrix} 0 & 1 & 0 & 0 & 0 \\ 8.8100 & 2 & 0 & 9.8100 & 0 \\ 0 & 0 & 1 & 0 & 0 \\ -6.9853 \cdot 10^{-4} & 6.9853 \cdot 10^{-4} & 0 & 0 & 9.3138 \cdot 10^{-4} \\ -1.1642 \cdot 10^{-4} & 1.1642 \cdot 10^{-4} & 0 & 0 & 1.3970 \cdot 10^{-3} \end{bmatrix}$$

(4.1)

$$\mathbf{A}_{y1} = \begin{bmatrix} 0 & 0 & 1 & 0 & 0 \\ 0 & 0 & 1 & 0 & 0 \\ 9.8100 & 0 & 0 & 9.8100 & 0 \\ 0 & 0 & 1.3970 \cdot 10^{-4} & 0 & 0 \\ 0 & 0 & 2.3284 \cdot 10^{-5} & 0 & 0 \end{bmatrix}$$

(4.2)

The same matrices computed in Delft3D are:

$$\mathbf{A}_{x1,\text{Delft3D}} = \begin{bmatrix} 0 & 1.0000 & 0 & 0 & 0 \\ 8.8097 & 2.0001 & 0 & 9.8098 & 0 \\ 0 & 0 & 1.0001 & 0 & 0 \\ -6.9828 \cdot 10^{-4} & 6.9859 \cdot 10^{-4} & 2.7937 \cdot 10^{-8} & 0 & 9.3135 \cdot 10^{-4} \\ -1.1639 \cdot 10^{-4} & 1.1644 \cdot 10^{-4} & 4.6564 \cdot 10^{-9} & 0 & 1.3970 \cdot 10^{-3} \end{bmatrix}$$

(4.3)

$$\mathbf{A}_{y1,\text{Delft3D}} = \begin{bmatrix} 0 & 0 & 1.0000 & 0 & 0 \\ 0 & 0 & 1.0001 & 0 & 0 \\ 9.8098 & 0 & 0 & 9.8098 & 0 \\ 0 & 0 & 1.3969 \cdot 10^{-4} & 0 & 0 \\ 0 & 0 & 2.3283 \cdot 10^{-5} & 0 & 0 \end{bmatrix}$$

(4.4)

The absolute value of the relative error in the norm of matrices $\mathbf{A}_x$ and $\mathbf{A}_y$ in Simulation 1 is equal to $2.3617 \cdot 10^{-5}$ and $1.8428 \cdot 10^{-5}$ respectively.

In Simulation 2, the sediment mixture is discretized in two sediment size fractions with characteristic grain sizes equal to 0.001 and 0.002 m. The sediment transport rate is computed using the Engelund and Hansen (1967) sediment transport relation. The sediment input at the upstream end of the fine and coarse size fractions is equal to 0 and $5.588 \cdot 10^{-5}~m^3/s$. This boundary condition is in equilibrium with a bed slope equal to $7.13541 \cdot 10^{-4}$ and a volume fraction content of the fine sediment in the active layer equal to 0. The volume fraction content of fine sediment in the substrate is equal to 1.

Under these conditions, matrix $\mathbf{A}_x$, Equation 3.13, and $\mathbf{A}_y$, Equation 3.14, (assuming no secondary flow) computed in Matlab are:

$$\mathbf{A}_{x2} = \begin{bmatrix} 0 & 1 & 0 & 0 & 0 \\ 8.8100 & 2 & 0 & 9.8100 & 0 \\ 0 & 0 & 1 & 0 & 0 \\ -4.6569 \cdot 10^{-4} & 4.6569 \cdot 10^{-4} & 0 & 0 & 9.3138 \cdot 10^{-4} \\ 4.6569 \cdot 10^{-4} & -4.6569 \cdot 10^{-4} & 0 & 0 & 9.3138 \cdot 10^{-4} \end{bmatrix}$$

$$(4.5)$$

$$\mathbf{A}_{y2} = \begin{bmatrix} 0 & 0 & 1 & 0 & 0 \\ 0 & 0 & 1 & 0 & 0 \\ 9.8100 & 0 & 0 & 9.8100 & 0 \\ 0 & 0 & 9.3138 \cdot 10^{-5} & 0 & 0 \\ 0 & 0 & -9.3138 \cdot 10^{-5} & 0 & 0 \end{bmatrix}$$

$$(4.6)$$

The same matrices computed in Delft3D are:

$$\mathbf{A}_{x2,\text{Delft3D}} = \begin{bmatrix} 0 & 1.0000 & 0 & 0 & 0 \\ 8.8097 & 2.0001 & 0 & 9.8098 & 0 \\ 0 & 0 & 1.0001 & 0 & 0 \\ -4.6426 \cdot 10^{-4} & 4.6655 \cdot 10^{-4} & 1.8624 \cdot 10^{-7} & 0 & 9.3135 \cdot 10^{-4} \\ 4.6426 \cdot 10^{-4} & -4.6655 \cdot 10^{-4} & -1.8624 \cdot 10^{-7} & 0 & 9.3135 \cdot 10^{-4} \end{bmatrix}$$

$$(4.7)$$

$$\mathbf{A}_{y2,\text{Delft3D}} = \begin{bmatrix} 0 & 0 & 1.0000 & 0 & 0 \\ 0 & 0 & 1.0001 & 0 & 0 \\ 9.8098 & 0 & 0 & 9.8098 & 0 \\ 0 & 0 & 9.3125 \cdot 10^{-5} & 0 & 0 \\ 0 & 0 & -9.3125 \cdot 10^{-5} & 0 & 0 \end{bmatrix}$$

$$(4.8)$$

The absolute value of the relative error in the norm of matrices $\mathbf{A}_x$ and $\mathbf{A}_y$ in Simulation 2 is equal to $2.3568 \cdot 10^{-5}$ and $1.8331 \cdot 10^{-5}$ respectively.

In Simulation 3, the sediment mixture is discretized in three sediment size fractions with characteristic grain sizes equal to 0.001, 0.002, and 0.004 m. The sediment transport rate is computed using the Meyer-Peter and Müller (1948) sediment transport relation with the hiding correction by Parker *et al.* (1982) with parameter b equal to 0.8 (Equation (2.20)). The sediment input at the upstream end of the fine, medium, and coarse size fractions is equal to $6.723 \cdot 10^{-5}$, $6.319 \cdot 10^{-5}$, and $5.865 \cdot 10^{-5}$ m^3/s. This boundary condition is in equilibrium with a bed slope equal to $7.13541 \cdot 10^{-4}$ and a volume fraction content of the fine and

medium fractions in the active layer equal to $1/3$. The volume fraction content of fine and medium fractions in the substrate is equal to $1/3$.

Under these conditions, matrix $\mathbf{A}_x$, Equation 3.13, and $\mathbf{A}_y$, Equation 3.14, (assuming no secondary flow) computed in Matlab are:

$$\mathbf{A}_{x3} = \begin{bmatrix} 0 & 1 & 0 & 0 & 0 & 0 \\ 8.8100 & 2 & 0 & 9.8100 & 0 & 0 \\ 0 & 0 & 1 & 0 & 0 & 0 \\ -1.2553 \cdot 10^{-3} & 1.2553 \cdot 10^{-3} & 0 & 0 & 2.0233 \cdot 10^{-3} & 1.2898 \cdot 10^{-3} \\ -9.2609 \cdot 10^{-6} & 9.2609 \cdot 10^{-6} & 0 & 0 & 3.1578 \cdot 10^{-3} & -1.1604 \cdot 10^{-4} \\ -5.1076 \cdot 10^{-7} & 5.1076 \cdot 10^{-7} & 0 & 0 & -1.4466 \cdot 10^{-4} & 3.0825 \cdot 10^{-3} \end{bmatrix}$$

(4.9)

$$\mathbf{A}_{y3} = \begin{bmatrix} 0 & 0 & 1 & 0 & 0 & 0 \\ 0 & 0 & 1 & 0 & 0 & 0 \\ 9.8100 & 0 & 0 & 9.8100 & 0 & 0 \\ 0 & 0 & 3.1510 \cdot 10^{-4} & 0 & 0 & 0 \\ 0 & 0 & 7.0133 \cdot 10^{-6} & 0 & 0 & 0 \\ 0 & 0 & 2.7599 \cdot 10^{-7} & 0 & 0 & 0 \end{bmatrix}$$

(4.10)

The same matrices computed in Delft3D are:

$$\mathbf{A}_{x3,\text{Delft3D}} = \begin{bmatrix} 0 & 1.0000 & 0 & 0 & 0 & 0 \\ 8.8097 & 2.0001 & 0 & 9.8098 & 0 & 0 \\ 0 & 0 & 1.0001 & 0 & 0 & 0 \\ -1.2549 \cdot 10^{-3} & 1.2553 \cdot 10^{-3} & 4.7001 \cdot 10^{-8} & 0 & 2.0232 \cdot 10^{-3} & 1.2898 \cdot 10^{-3} \\ -9.2611 \cdot 10^{-6} & 9.2605 \cdot 10^{-6} & 1.1237 \cdot 10^{-10} & 0 & 3.1590 \cdot 10^{-3} & -1.1600 \cdot 10^{-4} \\ -5.1066 \cdot 10^{-7} & 5.1063 \cdot 10^{-7} & 1.1737 \cdot 10^{-11} & 0 & -1.4453 \cdot 10^{-4} & 3.0833 \cdot 10^{-3} \end{bmatrix}$$

(4.11)

$$\mathbf{A}_{y3,\text{Delft3D}} = \begin{bmatrix} 0 & 0 & 1.0000 & 0 & 0 & 0 \\ 0 & 0 & 1.0001 & 0 & 0 & 0 \\ 9.8098 & 0 & 0 & 9.8098 & 0 & 0 \\ 0 & 0 & 3.1505 \cdot 10^{-4} & 0 & 0 & 0 \\ 0 & 0 & 7.0130 \cdot 10^{-6} & 0 & 0 & 0 \\ 0 & 0 & 2.7588 \cdot 10^{-7} & 0 & 0 & 0 \end{bmatrix}$$

(4.12)

The absolute value of the relative error in the norm of matrices $\mathbf{A}_x$ and $\mathbf{A}_y$ in Simulation 3 is equal to $2.3762 \cdot 10^{-5}$ and $1.8525 \cdot 10^{-5}$ respectively.

Deltares

Figure 4.2: *Pannerdensch Kop bifurcation (©Google Earth).*

4.3 2D test case

For the rapid development of the check of the well-posedness in the Hirano system, a real world test case near the Pannerdensche Kop is used. At this location the Bovenrijn bifurcates into the Waal heading west and the Pannerdensch Kanaal towards the north (see Figure 4.2).

The amount of sand transported into the Waal is about 8 times the amount of sand transported into the Pannerdensch Kanaal and the amount of gravel transport into the Waal branch equals 2 times the gravel transport into the Pannerdensch Kanaal (Frings *et al.*, 2014). This situation is therefore a suitable test for testing the well-posedness of the Hirano active layer equations.

Due to the fact that the implementation is not yet finished we cannot check this simulation.

5 Discussion and Further Research

The Jacobians computed in Delft3D and analytically are similar enough. A source of error is due not only to the fact that the derivatives in Delft3D are obtained with finite differences, but also due to the fact that the data used is not exactly the same. The values of the dependent variables in Delft3D differ from the imposed ones in the analytical computation because the simulation is not exactly a normal flow simulation. Thus, part of the difference between the analytical and the Delft3D solution is not error.

We have only tested the implementation in 3 cases which do not include all the generalities. For instance, we have to check with flow in both x and y or the effect of a curvilinear grid.

At this moment the only output are the Jacobians. It is necessary to implement the eigenvalues computation of the directional Jacobian, Equation 3.3, to obtain as an output the character of the system (i.e. hyperbolic or elliptic).

At this moment we use the sediment transport at the edges rather than at the cell centers. This is not a source of errors but a more consistent implementation would use the sediment transport at the cell centers (or the other variables at the cell edges).

In the current implementation the volume fraction content at the interface between the active layer and the substrate is obtained from the second layer of the Delft3D data structure. This second layer correctly corresponds to the top substrate layer if the bed degradation is smaller than the initial thickness of the second layer. A loop that identifies the top substrate layer in a general case needs to be implemented.

Secondary flow has not been studied. The matrix-vector formulation has not yet been checked and the implementation is not yet performed.

The role of the gravitational pull effects on the sediment transport has also not been studied. A thorough analytical study needs to be conducted before anything is implemented.

Mathematical analysis of the well-posedness of the Hirano active layer concept in 2D models

6 Conclusion

In the present report we present a mathematical analysis of the active layer model (Hirano, 1971) used in mixed-sediment river morphodynamics in combination with the Shallow Water Equations. This is relevant to assess the well-posedness of 2D simulations.

The criteria for well-posedness without considering the effects of secondary flow and slope effects have been formalized based on the continuous equations of motion. It is necessary to further study the effect of the neglected terms.

We obtain the system matrices using a symbolic solver. This allows us to plot the Monge cones to study the effect of the different model parameters. Moreover, this analytical solution allow us to validate the implementation of a well-posedness routine in Delft3D.

We have implemented a routine in Delft3D to characterize the system of equations (i.e. ill- or well-posed). The implementation appears to be correct. Yet, more tests need to be conducted.

A test case near the Pannerdensch Kanaal is created, which can be used to assess the occurrence of the elliptic behavior. When the eigenvalue computation has been validated it is recommended to research this graded sediment model for the occurrence of elliptic behavior, and what happens in the Delft3D solution when such a circumstance is encountered.

Mathematical analysis of the well-posedness of the Hirano active layer concept in 2D models

7 References

"Delft3D Hirano ellipticity check branch." URL https://svn.oss.deltares.nl/repos/delft3d/branches/research/TechnicalUniversityofDelft/20161020_ellipticity_check.

Blom, A., 2008. "Different approaches to handling vertical and streamwise sorting in modeling river morphodynamics." *Water Resour. Res.* 44 (3): W03415. DOI 10.1029/2006WR005474, ISSN 1944-7973, URL http://dx.doi.org/10.1029/2006WR005474. URL http://dx.doi.org/10.1029/2006WR005474.

Blom, A., G. Parker, J. S. Ribberink and H. J. de Vriend, 2006. "Vertical sorting and the morphodynamics of bed-form-dominated rivers: An equilibrium sorting model." *J. Geophys. Res., Earth Surface* 111: F01006. DOI 10.1029/2004JF000175, ISSN 2156-2202, URL http://dx.doi.org/10.1029/2004JF000175. URL http://dx.doi.org/10.1029/2004JF000175.

Blom, A., J. S. Ribberink and G. Parker, 2008. "Vertical sorting and the morphodynamics of bed form-dominated rivers: A sorting evolution model." *J. Geophys. Res., Earth Surface* 113: F01019. DOI 10.1029/2006JF000618, ISSN 2156-2202, URL http://dx.doi.org/10.1029/2006JF000618. URL http://dx.doi.org/10.1029/2006JF000618.

Blom, A., J. S. Ribberink and H. J. de Vriend, 2003. "Vertical sorting in bed forms: Flume experiments with a natural and a trimodal sediment mixture." *Water Resour. Res.* 39 (2): 1025. DOI 10.1029/2001WR001088, ISSN 1944-7973, URL http://dx.doi.org/10.1029/2001WR001088. URL http://dx.doi.org/10.1029/2001WR001088.

Chavarrías, V., G. Stecca, R. J. Labeur and A. Blom. "Ill-posedness in modelling mixed-sediment river morphodynamics." (in preparation).

Egiazaroff, I. V., 1965. "Calculation of nonuniform sediment concentrations." In *Proceedings ASCE*, vol. 91, pages 225–247.

Engelund, F. and E. Hansen, 1967. *Monograph on sediment transport in alluvial streams*. Tech. Rep., Hydraul. Lab., Tech. Univ. of Denmark, Copenhagen, Denmark.

Exner, F. M., 1920. "Zur Physik der Dünen." *Akad. Wiss. Wien Math. Naturwiss* 129(2a): 929–952. (in German).

Frings, R. M., R. Düring, C. Beckhausen, H. Schüttrumpf and S. Vollmer, 2014. "Fluvial sediment budget of a modern, restrained river: The lower reach of the Rhine in Germany." *Catena* 122 (0): 91–102. DOI 10.1016/j.catena.2014.06.007, ISSN 0341-8162, URL http://www.sciencedirect.com/science/article/pii/S0341816214001714. URL http://www.sciencedirect.com/science/article/pii/S0341816214001714.

Hirano, M., 1971. "River bed degradation with armouring." *Trans. Jpn. Soc. Civ. Eng* 3 (2): 194–195.

Hoey, T. B. and R. Ferguson, 1994. "Numerical simulation of downstream fining by selective transport in gravel bed rivers: Model development and illustration." *Water Resour. Res.* 30 (7): 2251–2260. DOI 10.1029/94WR00556, ISSN 1944-7973, URL http://dx.doi.org/10.1029/94WR00556. URL http://dx.doi.org/10.1029/94WR00556.

Kalkwijk, J. P. T. and R. Booij, 1986. "Adaptation of secondary flow in nearly-horizontal flow." *J. Hydraul. Res.* 24 (1): 19-37. DOI 10.1080/00221688609499330, URL http:

//dx.doi.org/10.1080/00221688609499330. URL http://dx.doi.org/10.1080/00221688609499330.

Meyer-Peter, E. and R. Müller, 1948. "Formulas for bed-load transport." In *Proc. 2nd Meeting Int. Assoc. Hydraul. Struct. Res.*, pages 39–64. Stockholm.

Parker, G., 1991. "Selective Sorting and Abrasion of River Gravel. I: Theory." *J. Hydraul. Eng.* 117 (2): 131–147. DOI 10.1061/(ASCE)0733-9429(1991)117:2(131), URL http://ascelibrary.org/doi/abs/10.1061/%28ASCE%290733-9429%281991%29117%3A2%28131%29. URL http://ascelibrary.org/doi/abs/10.1061/%28ASCE%290733-9429%281991%29117%3A2%28131%29.

Parker, G., P. C. Klingeman and D. G. McLean, 1982. "Bedload and size distribution in paved gravel-bed streams." *Journal of the Hydraulics Division* 108 (4): 544–571.

Ribberink, J. S., 1987. *Mathematical modelling of one-dimensional morphological changes in rivers with non-uniform sediment.* Ph.D. thesis, Delft University of Technology, The Netherlands.

Saint-Venant, A. J. C. B., 1871. "Théorie du mouvement non permanent des eaux, avec application aux crues des rivières et à l'introduction des marées dans leur lit." *Comptes Rendus des séances de l'Académie des Sciences* 73: 237–240. (in French).

Sieben, A., 1994. *Notes on the mathematical modelling of alluvial mountain rivers with graded sediment.* Tech. Rep. 94–3, Delft University of Technology.

Sieben, J., 1997. *Modelling of hydraulics and morphology in mountain rivers.* Ph.D. thesis, Delft University of Technology.

Sloff, C. J., 1992. *The method of characteristics applied to analyse 2DH models.* Tech. Rep. 92–4, Delft University of Technology.

Stecca, G., A. Siviglia and A. Blom, 2014. "Mathematical analysis of the Saint-Venant-Hirano model for mixed-sediment morphodynamics." *Water Resour. Res.* 50: 7563–7589. DOI 10.1002/2014WR015251, ISSN 1944-7973, URL http://dx.doi.org/10.1002/2014WR015251. URL http://dx.doi.org/10.1002/2014WR015251.

Viparelli, E., R. R. H. Moreira and A. Blom, 2016. "Modelling stratigraphy-based GBR morphodynamics." In *Proc. Gravel Bed Rivers 8, Kyoto, Japan.* In press.

A Changes to Delft3D

A branch of the Delft3D modelling system was created for the development of the approximate eigenvalue analysis (url). Using a branch allows the implementation of new concepts, whilst ensuring the stability of the main development line. The following files have been updated for the implementation of the check of the well-posedness of the active layer description of Hirano (1971), and subsequently determine the possibilities to circumvent the occurrence of elliptic behavior.

```
engines_gpl/flow2d3d/packages/data/include/inttim.igs
engines_gpl/flow2d3d/packages/data/src/basics/globaldata.f90
engines_gpl/flow2d3d/packages/io/src/input/rdsedmortra.f90
engines_gpl/flow2d3d/packages/io/src/output/wrsedm.f90
engines_gpl/flow2d3d/packages/kernel/kernel.vfproj
engines_gpl/flow2d3d/packages/kernel/src/compute_sediment/erosed.f90
engines_gpl/flow2d3d/packages/kernel/src/compute_sediment/hirano_check.f90
engines_gpl/flow2d3d/packages/kernel/src/compute_sediment/hirano_check_init.f90
engines_gpl/flow2d3d/packages/kernel/src/compute_sediment/hirano_check_perturbation.f9
engines_gpl/flow2d3d/packages/kernel/src/compute_sediment/Makefile.am
engines_gpl/flow2d3d/packages/kernel/src/compute_sediment/rg_dependencies.f90
engines_gpl/flow2d3d/packages/kernel/src/main/trisol.f90
engines_gpl/flow2d3d/packages/manager/src/tricom_step.F90
utils_gpl/morphology/packages/morphology_data/src/morphology_data_module.f90
utils_gpl/morphology/packages/morphology_io/src/rdmor.f90
utils_gpl/morphology/packages/morphology_io/src/rdstm.f90
utils_gpl/morphology/packages/morphology_kernel/src/bedcomposition_module.f90
```

In addition output fields 'HIRCHK', 'HIRJCU', 'HIRJCV' are added to 'map-sed-series' in the trim-file. The field 'HIRCHK' is used to indicate whether the approximate eigenvalues at the time step previous to writing the map file are elliptic or not. This is indicated using a 1 for elliptic and 0 for not elliptic. The fields 'HIRJCU', 'HIRJCV' represent the approximate Jacobian in u and v direction. This check can be activated using the 'HiranoCheck' option in the morphology input file (with file extension .mor). For ease of use, the output has been added in such a way that it can be viewed and loaded into Matlab memory using Delft3D-QuickPlot. Furthermore the perturbation can be added using the keyword 'HiranoCheckPertubation'

```
[Numerics]
    HiranoCheck = 1      [ - ] Flag for well-posedness of Hirano (1971) check
                              0 (default): Off
                              1          : On
    HiranoCheckPertubation = 0.0001     # (default 0.0001)
```